Quality Evaluation of Wing Sections Obtained with Different Manufacturing Techniques

João N. M. F. S. Gomes
Departamento de Ciências Aeroespaciais
Universidade da Beira Interior
Calçada Fonte do Lameiro, 6200-001 Covilhã
E-mail: Jonny_1421@outlook.pt

Abstract

The performance of small aerial vehicles is dependent of the aerodynamic characteristics of the airfoil employed in its wings. Not only the chosen airfoil should perform well for low Reynolds numbers but the manufacturing concepts should be carefully selected and executed to obtain a good surface quality. This work aims to investigate the impact of five different structural concepts and the relative manufacturing techniques, typically used in UAV wings, on the aerodynamic response. Five structural concepts were selected for this study, those are: foam; foam covered with fiberglass; fiberglass skin with balsa core; balsa; foam covered with fiberglass box. Three similar rectangular shaped wing panels of 350 mm chord and 200 mm span were built per concept using the same airfoil shape. All manufactured wing panels were subdued to a laser scanning process to obtain the respective 3D models, then seven equally spaced wing profiles were extracted from each model. Each profile geometry were converted to text files compatible with XFLR5 software. All geometries and aerodynamic responses were compared with the original airfoil's data.

1. Introduction

The first step to consider when designing a wing is to choose or even create an airfoil based on the optimal aerodynamic characteristics for a specific flight envelope. However there are always small deviations between the designed dimensions and the manufactured part, no matter how meticulous and careful the manufacturing process is performed. It is not always possible to predict and justify these geometry deviations, they can occur for a number of non-controllable reasons like: excess of sanding to smooth specific areas; inappropriate use of working tools; using a machine that is not calibrated correctly among others. The geometry differences between the pre-designed conditions and the real wing shape can lead to undesirable changes in the aerodynamic characteristics.

The airfoil chosen to perform this evaluation was similar to the one used in the development of a LEEUAV wing [1], with the difference that this only has 10% t/c relative thickness.

This study is divided into three distinct parts: establishing the details and execution of the manufacturing process of each structural concept; the laser scanning and post process applied to obtain the wing panels' 3D models and the seven wing profile shapes; the evaluation and comparison of the geometry and aerodynamic response of each wing profile with the respective airfoil data. This study has different intentions and purposes; identify and amend possible manufacturing process steps; verify the aerodynamic behavior along the span and check if the performance is consistent for different wing panels of the same structural concept; identify the structural concept that more accurately resembles the airfoil's geometry and aerodynamic performance. For more details related with this work the reader should consult ref. [2].

2. Manufacturing methodology

The foam wing panel concept consists of a rigid foam wing shaped body with two 5×10 mm slots to fit 2 rectangular pine spars. This wing panel was cut from a foam block and a G-code was generated from Profili software for this purpose. The wing characteristics were specified in Profili [3] using the *Wing Panel Management* window as follows:

Geometry characteristics: – Rectangular wing; chord size of 365 mm; span size of 200 mm; the airfoil coordinates; the slot dimension and position (30% chord).

Cutting parameters: Block dimensions 200×600 mm; kerf 0.4 mm; Feed rate of 160

mm/min; electric current intensity of 1.3 Ω; voltage set to 37 V.

A G-code was extracted from profile according with the cutting settings and imported into the CNC hot-wire, were the cut was performed. The optimum cut was established automatically and the path starts by cutting the upper slot returning to the initial position outside the block, then it contours the wing starting from the upper surface's trailing edge and contours the hole wing. The pine spars were cut according to the slot's dimensions and then glued with epoxy resin. All wing surface was paint for scanning texture purposes using appropriate foam ink supplied in pressurized canisters.

The foam covered with fiberglass concept follows the same manufacturing methodology as the foam concept with the distinction applied to the cutting settings. Since the wing panel was to be covered in fiberglass the thickness of the fiberglass composite needed to be evaluated to be accounted to the design. A fiberglass palte of 100×100 mm was built for this purpose and the mean thickness was found to be 0.45 mm. The fiberglass fabric used has 200 g/cm^3 and is common to all concepts that required fiberglass in its structures. The cutting settings are similar to the foam concepts with the difference in wing chord and kerf width specified to be 355 mm and 1 mm respectively. Three hand lamination methods were elaborate for quality improvement purposes. The first method consists on a horizontal lamination of each surface with the other resting on the negative mold casing. The wing was to be revolved with one single fiberglass sheet. Resin was applied and spread on the foam surface to prevent the undesired shifting of the fiber roving's orientation. The fabric was applied over the surface, covered with more resin and then coated with a plastic sheet. The wing was revolved to laminate the second surface. The leading edge was revolved by stretching the plastic sheet with the fiberglass already impregnated with resin. The second side was then covered in the same procedure, with the fiberglass uniting in the trailing edge of each surface. The resin and trapped air bubbles were drained by passing a plastic spatula over the plastic on the chord direction. The resin was allowed to cure at room temperature for 24 hours. The resin cure is similar to all concepts.

The second lamination method is similar but it was performed with the wing resting vertically on a stand. The third lamination was performed just like the first but the wing was left to cure inside a closed foam mold pre-covered with plastic sheet. The excess fiberglass fabric was cut from the wing panels sides. The chord length was measured and marked to trim the excess composite from the trailing edge. All wing panels that have fiberglass acting as the wing skin were painted using an enamel based ink for surface detection purposes of the laser scanning process.

The fiberglass skin with balsa core concept was designed in Catia v5 [4]. The concept consists of an inside structure that has 4 equally spaced balsa ribs designed to fit into a rectangular plywood spar and an outside surface of two fiberglass composite acting as the wing skin. The ribs and spar have 3 mm rectangular slots at 25% chord to allow the connection. The ribs were designed with an offset of 0.45 mm to account for the fiberglass skin's mean thickness. Both ribs and spar were cut into shape using a CNC laser machine from 3 mm sheets of the respective material and then assembled and glued using cyanoacrylate glue. The fiberglass skins required two rigid molds to sustain the high pressures applied by a vacuum bag technique by preserving the airfoil shape of both airfoil surfaces; Sikablock M700 model board [5] was used to produce the molds. The molds were designed with 450 mm length and 300 mm span in Catia V5 and were post process in Deskproto 6.1 [6] to obtain a CNC milling *G-code* for the toolpath generation of the router machine according to the specifications of the tools and cutting setting. The molds have 50 mm flat extremities and 100 mm excess length in span to drain resin and facilitate the lamination. The wing's skins were glued to the inside structure using epoxy resin and the molds were closed acting as a pressure vessel. The wings were extracted from the closed mold the following day and paint was applied.

The balsa concept was designed in Catia V5 and consists of several elements: one rigid balsa body of 15 mm length in chord direction consistent with the airfoil's leading edge shape; four 2 mm thick balsa ribs equally spaced from each other with three slots, one to fit the spar and the other two to glue a 1mm balsa sheet in both surfaces between the leading edge body and the spar, in order to close the wing panel; a rectangular spar made from plywood; a 50 mm length rigid body made from balsa has designed with slots to fit the end side of the ribs consistent with the trailing edge shape of the airfoil. The rigid bodies were saved in STL format to be processed for a two side milling in the CNC router. The ribs and spar were saved in a DFX format and were processed in Lasercut [7] software to be cut by the CNC laser machine just like in the previous concept. The balsa sheets were cut by hand according to the slots designed for both surfaces. All elements were assembled in the lower surface foam mold. All elements

were connected and glued using cyanoacrylate glue. To the wing panels has applied a SolarFilm [8] thermo plastic cover to close the hollow spaces of the structure and give a smother surface finish.
The foam core with fiberglass box concept was also designed in Catia V5 its structure consists of: a 25% chord long rigid foam body covered with fiberglass with the airfoil leading edge shape with one rectangular slot in each side; two rectangular pine spars just like the ones used in the first two concepts; four equally spaced ribs designed to be glued to the leading edge body rear flat side end; a trailing edge rigid body equal to the one used in the balsa wing concept. The leading edge foam body needed to be cut from a foam block, so the DFX file that contains its geometry was imported into Devfoam [9] software were the cutting path was defined and the NC-program exported, according with the following cutting settings: electric current intensity of 1.3 Ω; voltage of 37 V; mean velocity of 160 mm/min; kerf width set to 2 mm. The foam block was cut in the CNC hot wire and the pine spars were glued to its slots with epoxy resin. The body was prepared for two partial hand laminations. The first consists on the coverage of the spars and vertical side, the second revolves the foam body the upper spar to the end of the lower spar. The foam that did not require fiberglass reinforcement was covered with plastic tape to prevent the resin from flowing to unnecessary parts of the wing, making it unnecessarily heavier. The second lamination was performed using a low pressure vacuum bagging process. After the resin cure time the body was sanded to give an overall smooth surface. All components were assembled in the lower surface foam mold. The ribs were glued to the flat side of the leading edge body using 10 minutes epoxy glue. The rear end of the ribs were connected to the trailing edge body slots and glued with cyanoacrylate. The wing panel was covered with Oracover [10] thermo plastic for the same purposes of the balsa concept.

3 Laser scanning methodology

The laser scanning process was developed with an Artec spider [11] laser scanner and the scanned data was post processed on Artec Studio 9 software [12]. Markers were inserted on all wing panels using a magic marker to provide references for the alignment of the different scans. The wings covered in thermoplastic cover had to be coated with an anti-glare spray because they were still reflective, making the surface detection more difficult and it generates more *noise*. The paint used in the concepts covered with fiberglass was mate, not glossy, to prevent light reflection. The scanning process was executed using the *geometry+texture* mode. The scanning settings were maintained as default and the scanner was set to 8 fps which was enough to ensure the overlapping of adjacent frame areas as the scanner was moved. The brightness of the scanner was set according with the surface of each structural concept using the *preview mode*. The remaining settings were maintained default just as recommended. The wing panels were scanned by sections in the following sequence:

1. Upper surface
2. Partial area of the upper surface leading edge
3. Edge formed by the upper surface and the right rib
4. Edge formed by the upper surface and the left rib
5. Right rib
6. Left rib
7. Edge formed by the lower surface and the right rib
8. Edge formed by the lower surface and the left rib
9. Lower surface
10. Partial area of the lower surface leading edge

The first 4 scans represents the upper surface, the last 4 scans represents the lower surface while scans 5 and 6 represents the laterals of the wing panels. Scans 3, 4, 7 and 8 were necessary to align the lateral scans, without them we were selecting points from different planes to align with each other.
The scans post processing took the following sequence: erase the surroundings; alignment of the scans; global registration; noise removal; fusion of the scans; flaws rectification; mesh simplification; map texture.
The unwanted elements captured in the scanning process were deleted using the appropriate option of the *eraser tool*.
The alignment was performed individually, in the same order they were scanned. Multiple common points were selected in pairs using the references to establish the correct bound, the texture align feature was enabled to allow texture features to assist the alignment.
After scanning, the software contains no information about the relative position of the multiple scans. To assemble the scans together into a single model, the data must be converted into a single coordinate system. To convert the scans into a single coordinate system the *global registration* algorithm was applied.
During scanning some unwanted features called *outliers* appeared. These are small surface or points not connected to the main surface and

can spoil the model by producing unwanted fragments in the *fusion* algorithm. All processed data was fused into a single polygonal 3D model using the *fast fusion* algorithm. All the following algorithms were applied to the resulting polygonal mesh: - the *hole filling and edge smoothing* with the intention of filling small gaps; - the *smoothing* algorithm with the purpose of smoothing noisy areas although some still remained; - *Mesh simplification* algorithm with the intention of reducing the memory space occupied by reducing the number of elements composing the mesh, this was essential for the normal function of other software packages for the development of posterior tasks. The wing panels were re-positioned using the *positioning tool*, so that the left rib would be set adjacent to one of the coordinate plane. The leading edge point could not be placed coincident with the origin of the coordinate system.

The mesh was saved in STL format and was imported into Meshmixer software [13] were the geometry was submitted to a slicing operation. This operation divided the wing panels into 1 mm sections (slices) along the span direction, were seven equally spaced slices were selected to be exported. The slices were exported in OBJ format and imported into Catia V5 using the *existing component* feature of the *assembly design* module. The OBJ file was converted into a Cat product by attributing an offset of 0 mm in the *digital mockup* of the *DMU optimizer* module which was saved in Model format. The file was opened, copied and pasted into the *part design* module. A plane was inserted parallel to the slice, and the points were selected and projected to the plane from the trailing edge to the leading edge direction defining the upper surface contour, and from the leading edge back to the trailing edge defining the lower surface contour. The points were exported from Catia V5 into a text file format using the Aerospace Profile Modeler application. The application exports the points in the same sequence as they were selected. All slices coordinates were obtained by this iterative process, which applied to all structural concepts took some time. Since the slices were not properly positioned in the coordinate system, all coordinates were imported into Excel were a series of transformations (rotation and translation) were performed so that the slices could be compared to the airfoil's geometry. With the slices position established, all points were divided by the wing chord. The upper surface suffered a mirror operation around the *y*-axis, so that the upper surface would be displayed for the negative values of the x-axis, from the leading to the leading edge direction. The new coordinates were saved into new text files for the geometry analysis.

5. Geometry analysis

To perform a geometry comparison between the obtained slice shapes and the airfoil's, the slices should have identical *x*-coordinates in order to calculate the difference between the respective *y*-coordinates. But the coordinates exported from Catia V5 into text files were randomly obtained. It was required to interpolate the *y*-coordinates of the required x-positions of the slice points, to find the correspondent *y*-coordinates of the airfoil. A Matlab [14] routine was written to read the coordinates text files of both slices and airfoil and arranged them in columns. The interpolation function intrinsic to Matlab (function = *interp*) was used specifying the data accordingly and the method was set to be the spline interpolation. The code generates the new *y*-coordinates of the airfoil and then calculates the difference between the y-coordinates of the slice and the respective interpolated airfoil coordinates. The remaining code is for plot purposes, were the results are displayed in several graphs. Two graphs were saved per slice: one to display the geometry of the slice compared to the airfoil and the other to display the relative thickness absolute and relative errors along the chord direction.

4. Aerodynamic analysis

The aerodynamic analysis was performed in XFLR5 software [15]. XFLR5 is an analysis tool for airfoils, wings and planes operating at low Reynolds numbers. XFLR5 only recognizes plain traditional data format containing the *x*- and *y*-coordinates of the airfoils, which must be organized from the trailing edge round the leading edge and back to the trailing edge on any direction. This was the reason why the coordinates were extracted from Catia V5 in the sequence described. The slices were open one at a time and a *global refinement* was applied to set the number of panels to 200. This divides and distributes the number of points evenly throughout the upper and lower surfaces. All seven slices of a wing panel were opened and analyzed together. The analysis settings was described in the *batch foil analysis* window as follows: all slices imported were selected from the *foil list* to be subdued to the analysis, the *type one* analysis was selected; the *transition* was left as default in the trailing edge; the *Ncrit* value was set to 9 to approximate the simulation performed on average wind tunnels; the operating conditions were set on the *list* window were the Reynolds numbers were specified to 140,000, 340,000 and 600,000; the angle of

attack was set to range between -5 and 15 with 1 degree increment. The analysis intention was to verify the behavior of the aerodynamic coefficient obtained for each slice with those obtained for the original LEEUAV airfoil. With the aerodynamic analysis complete the aerodynamic coefficient curves of each wing panel were exported in text format, for plot purposes in Matlab and to access specific aerodynamic information in Excel. The aerodynamic curves evaluated were: Lift coefficient; Drag coefficient; Pitching moment coefficient; Drag polars; and the transition positions of the upper and lower surfaces.

The aerodynamic information captured from Excel was: the zero angle of attack lift coefficient (Cl_0); maximum lift coefficient (Cl_{max}) and the corresponded angle of attack (α_{Clmax}); minimum drag coefficient (Cd_{min}) and the corresponded angle of attack (α_{Cdmin}) and lift coefficient (Cl_{Cdmin}); the maximum lift-to-drag coefficient $(Cl/Cd)_{max}$ and the correspondent angle of attack ($\alpha_{(Cl/Cd)max}$).

6. Results

Only the first wing panels' slices geometry comparison graphs (left side's shape) of each structural concept are presented (Figure 1 to 7) except for the case of the balsa concept and the foam and fiberglass box concept due to larger geometry deviations of the halfway slices located between ribs. In this section the slices lose camber due to the concave shape that the thermo-plastic makes in the hollow space (second slice).

The results obtained from the geometry analysis can be interpreted as changes in geometry features of the airfoil like: camber; relative thickness as their maximum positions (Table 2 to 6). The chord length of each slice is different along all wing panels' span (Table 1), which produces different geometry results and consequently different aerodynamic response along the wingspan. This variation in chord length is due to the laser scanning process incapability of detecting the low thickness of the trailing edge end. The wing panels' upper and lower surfaces did not unite in the trailing edge after the alignment, originating a small gap that was filled with the *hole filling* algorithm leaving small deformations in the surrounding area.

Graph 1 to 25 display the aerodynamic results obtained for the first wing panel of all structural concepts for the condition of Re = 140,000. The results displays a reduction of lift coefficient for all angles of attack but it is more evident for higher angles, so the maximum lift coefficient is lower than the airfoil's and the stall angles is increased 2 to 3 degrees for most slices. It was verified that the drag coefficient is higher for lower angles of attack and lower for higher angles of attack. This is due to an increase of friction drag due to the increase of the slice's relative thickness and a decrease of pressure drag due to lower adverse pressure gradients in the pressure recovery region of the upper surface. The airfoil has good longitudinal stability response because the pitching moment coefficient is negative for all angle of attack, this means that it creates a moment that tends to rotate the airfoil nose down. As the angle of attack increases, the pitching moment loses some magnitude but it still remains negative. The slices pitching moment coefficient is more positive compared with the airfoil's due to two reasons; first the lift created due to the pressure differential between the upper and the lower surfaces has a lower magnitude; secondly because the pressure distribution along the chord is different than the airfoil's and the trailing edge section force distribution is not as great to counter-balance the leading edge's and the center of pressure is moved forward.

The transition behavior between most slices is very similar to the airfoil's, but the transition moves forward faster for lower lift coefficients. Since all slices have higher differences in geometry on the trailing edge, making it thinner, the pressure gradient is increased which causes the earlier transition and consequently an increase of friction drag. The most evident transition changes are verified for hallway slices located between ribs of the wings covered with heat shrink plastic film. In these slices for $-3^\circ < \alpha < 0^\circ$ there is a huge forward displacement of the transition location, so the turbulent layer develops sooner increasing the friction drag for low range of angles of attack. The remaining slices have a similar transition curve compared with the original airfoil, but the transition starts sooner in chord length direction and for lower values of lift coefficient.

Table 7 to 11 show a comparison between the airfoil and the average aerodynamic results calculated from all wing panels for all flow conditions. Table 12 summarizes the overall concepts that provided the best performance approximation relating to the airfoil's aerodynamic parameters. This table is independent of the Reynolds number, it is provided by the average results obtained for all slice's and Reynolds numbers.

Conclusions

The aerodynamic performance results show that some structural concepts provide closer results to the original airfoil's in maximum lift coefficient while others are better in minimum

drag, indicating that there is not one single concept with an overall better representation in all aerodynamic parameters.
As for the laser scanning process it was impossible to obtain an accurate representation of all wing panels' trailing edges, due to the incapacity of the scanner to capture thin surfaces. Since one of the main purposes of this work was to find possible ways of improving the accuracy of the manufacturing process, by the evaluation of the systematic errors found in the several manufacturing concepts, even small deviations could lead to a wrong correction of some manufacturing process procedures.
It is possible that the results obtained for the fiberglass skin with balsa core concept could be more accurate than the one displayed, due to difficulties in the manufacturing technique of the fiberglass skins molds.
This work provides an insight on the geometry variations of the different structural concepts and can be taken in account for future wing projects.

References

[1] L. F. V. Cândido, "Projeto de um UAV Solar de Grande Autonomia," MSc Thesis, Universidade da Beira Interior, Covilhã, October, 2014.

[2] J. N. Gomes, "Quality Evaluation of Wing Sections Obtained with Different Manufacturing Techniques," MSc Thesis, Universidade da Beira Interior, Covilhã, 2016.

[3] DevCad Team, "Profili 2.0," June 2015. [Online]. Available: http://www.profili2.com/eng/default.asp. .

[4] Dassault Systèmes, "V5 Portfolio - Dassault Systèmes," [Online]. Available: http://www.3ds.com/products-services/catia/products/v5/portfolio/. [Acedido em June 2015].

[5] Sika, "SikaBlock® Milling Parameters - Sika Deutschland GmbH," [Online]. Available: file:///C:/Users/Jo%C3%A3o%20Nuno/Downloads/Sika_2010_10_Broschuere_Fraesdaten_fuer _web_eng.pdf. . [Accessed June 2015].

[6] Delft Spline Systems, "Deskproto Reference Manual," 1995, 2013. [Online]. Available: http://www.deskproto.com/files/dp61refman.pdf.. [Acedido em June 2015].

[7] graham wideman, "LaserCut -- Software overview," [Online]. Available: http://grahamwideman.wikispaces.com/LaserCut+--+Software+overview. [Acedido em June 2015].

[8] Solarfilm, "Solar Film," [Online]. Available: http://www.solarfilm.co.uk/default.aspx. [Acedido em June 2015].

[9] DevCad, "DevFoam, 4 axis hot wire foam cutting CNC," [Online]. Available: http://www.devcad.com/eng/devfoam.asp. [Acedido em June 2015].

[10] burburhobbies, "ORACOVER COVERING MATERIAL - Home," [Online]. Available: https://www.burburhobbies.com/products/95/pilot-rc-parts/oracover-covering-material. [Acedido em June 2015].

[11] Artec Group, "[PDF]Artec Spider Product Specifications - Central Scanning," [Online]. Available: http://www.central-scanning.co.uk/pdf/Artec-Spider-Product-Specifications.pdf. [Acedido em June 2015].

[12] "Artec Studio User Guide - Artec Group," [Online]. Available: http://artec-group.com/sw/ug/ug.pdf. [Acedido em June 2015].

[13] Autodesk, "Meshmixer," [Online]. Available: http://www.meshmixer.com/. [Acedido em June 2015].

[14] Mathworks, "MATLAB - The Language of Technical Computing," [Online]. Available: http://www.mathworks.com/products/matlab/. . [Acedido em June 2015].

[15] " XFLR5 Analysis of foils and wings operating at low Reynolds numbers," [Online]. Available: https://engineering.purdue.edu/~aerodyn/AAE333/FALL10/HOMEWORKS/HW13/XFLR5_v6.01_Beta_Win32(2)/Release/Guidelines.pdf.. [Acedido em June 2015].

Table 1. Number of points and chord length defining each slice.

Tecniques of construction	Slices / Wings	N° of points defining spline							Chord lenght [cm]						
		1	2	3	4	5	6	7	1	2	3	4	5	6	7
1-FOAM	1	379	223	401	436	301	355	349	347,6	348,7	348,5	348,6	350,2	349,4	347,1
	2	436	465	483	465	496	635	497	348,9	350,0	349,3	350,2	350,2	351,2	350,2
	3	696	500	536	701	533	613	494	348,9	350,0	349,3	350,0	350,2	351,2	350,2
2-Foam+Fiberglass coat	1	384	394	508	399	392	380	348	350,4	350,5	350,2	351,3	351,1	351,2	350,3
	2	475	510	366	387	410	392	413	350,1	351,8	351,3	350,9	351,0	350,6	351,0
	3	298	311	366	309	330	304	368	350,1	349,8	349,8	350,1	349,8	350,5	349,9
3-Fiberglass Skin	1	434	402	405	444	436	439	471	352,1	351,5	351,9	351,5	352,1	351,0	352,4
	2	331	385	398	451	395	420	399	347,6	350,3	350,8	350,4	350,0	350,3	348,9
4-Balsa	1	124	107	95	108	125	125	142	347,8	348,8	349,4	348,5	349,9	350,0	348,8
	2	442	316	392	324	380	383	421	345,7	347,4	347,3	347,3	347,9	348,0	348,4
	3	312	275	331	305	323	342	357	347,9	347,9	348,1	349,2	348,7	349,1	348,6
5-Fiberglass box	1	359	476	356	424	367	415	373	349,3	347,8	350,3	350,8	351,2	351,8	352,1
	2	366	386	382	304	324	291	408	350,4	349,5	350,3	350,0	350,0	349,9	350,7
	3	597	324	362	345	368	361	696	349,4	349,0	349,2	348,8	349,3	349,9	351,1

Table 2. Geometry characteristics of each slice of the foam wing panels displayed in percentage.

		thickness (y/c)	max.thickness position(x/c)	max camber	max camber position
WING 1	Slice1	9.95	24.41	5.36	48.31
	slice2	10.11	25.5	5.31	47
	slice3	10.15	26	5.29	48.2
	slice4	10.15	26.1	5.26	47.3
	slice5	10.13	26.3	5.18	47.4
	slice6	10.18	25.9	5.18	48.4
	slice7	10.27	26.1	5.13	48.4
WING 2	Slice1	10.07	24.1	4.91	46.2
	slice2	10.17	26.2	4.97	47.3
	slice3	10.17	26	4.85	46.2
	slice4	10.12	25.5	4.87	47.5
	slice5	10.13	24.8	4.81	45.8
	slice6	10.10	26.4	4.84	47.4
	slice7	10.10	26.4	4.82	46.9
WING 3	Slice1	10.27	26.1	5.45	48.9
	slice2	10.32	25.30	5.44	49.4
	slice3	10.36	25.4	5.41	49.1
	slice4	10.41	0,25	5.34	50.2
	slice5	10.42	25.8	5.28	48.6
	slice6	10.39	25.6	5.2	47.9
	slice7	10.36	25.7	5.15	45.7
	Airfoil	10	24,8	5,23	48,1

Table 3. Geometry characteristics of each slice of the foam covered with fiberglass displayed in percentage.

		thickness (y/c)	max.thickness position(x/c)	max camber	max camber position
WING 1	Slice1	10.07	24.2	4.92	47.1
	slice2	10.08	24.5	5.08	49.2
	slice3	10.11	25.7	4.99	47.4
	slice4	10.09	25.8	5.21	48.3
	slice5	10.14	26.1	5.16	48
	slice6	10.11	25.2	5.15	48.1
	slice7	10.09	25.4	5.08	47.8
WING 2	Slice1	10.11	24.2	4.93	45.9
	slice2	10.09	26.4	4.96	48
	slice3	10.10	26.3	4.95	47
	slice4	10.11	25.9	5.11	47.4
	slice5	10.12	26	5.06	45.6
	slice6	10.19	25.6	5.09	46.2
	slice7	10.25	25.1	5.24	51.8
WING 3	Slice1	10.27	26.1	5.45	48.9
	slice2	10.32	25.30	5.44	49.4
	slice3	10.36	25.4	5.41	49.1
	slice4	10.41	0,25	5.34	50.2
	slice5	10.42	25.8	5.28	48.6
	slice6	10.39	25.6	5.2	47.9%
	slice7	10.36	25.7	5.15	45.7
	Airfoil	10	24,8	5,23	48,1

Table 4. Geometry characteristics of the fiberglass skin with balsa core displayed in percentage.

		thickness (y/c)	max.thickness position(x/c)	max camber	max camber position
WING 1	Slice1	10.08	25.5	5.31	47.4
	slice2	10.18	23.9	5.38	47.6
	slice3	10.13	24.5	5.36	47.1
	slice4	10.13	24.4	5.37	47.6
	slice5	10.11	24.2	5.25	48.7
	slice6	10.17	24.5	5.33	48.5
	slice7	10.08	25.7	5.31	46.9
WING 2	Slice1	10.52	24.4	5.15	47.8
	slice2	10.43	23.4	5.13	48.6
	slice3	10.4	23.7	5.08	48.5
	slice4	10.37	24.2	5.07	48.5
	slice5	10.41	24.6	5.01	48.1
	slice6	10.38	24.1	5.13	48.5
	slice7	10.41	24.3	5.04	47.1
	Airfoil	10	24,8	5,23	48,1

Table 5. Geometry characteristics of each slice of the balsa wing panels displayed in percentage.

		thickness (y/c)	max.thickness position(x/c)	max camber	max camber position
WING 1	Slice1	9.75	24.3	4.87	41.3
	slice2	9.55	25.3	4.32	39.2
	slice3	9.45	20	4.78	44.4
	slice4	9.39	19.9	4.27	40.5
	slice5	9.34	25	4.62	43.3
	slice6	9.25	24.8	4.28	42
	slice7	9.42	24.2	4.64	43.1
WING 2	Slice1	10.07	24.09	5.27	49.5
	slice2	10.01	24.8	4.88	48.6
	slice3	10.04	23.5	5.33	47.7
	slice4	10.08	24.3	4.73	45.8
	slice5	10.06	22.6	5.11	45.5
	slice6	10.01	24.5	4.6	44.2
	slice7	9.99	24.9	5.11	47.6
WING 3	Slice1	10.02	24.8	4.97	49.1
	slice2	9.94	25.2	4.49	41.2
	slice3	9.99	24.4	4.96	46.5
	slice4	9.95	25.1	4.44	42.8
	slice5	9.98	24.9	4.74	47
	slice6	9.94	25.6	4.36	43.7
	slice7	10	25.1	4.85	45.7
	Airfoil	10	24,8	5,23	48,1

Table 6. Geometry characteristics of each slice of the foam wing panels displayed in percentage.

		thickness (y/c)	max.thickness position(x/c)	max camber	max camber position
WING 1	Slice1	9.97	21.3	5.6	48.3
	slice2	9.97	24.2	5.12	46.8
	slice3	9.82	24.7	5.39	49.1
	slice4	9.84	24.6	5.27	46.6
	slice5	9.86	24.9	5.66	48.6
	slice6	9.92	23.8	5.24	48.1
	slice7	10.11	23.5	5.6	49.1
WING 2	Slice1	10.03	20.5	4.87	42.9
	slice2	10.16	20.2	4.52	39.5
	slice3	10.07	20.5	5.03	47.2
	slice4	10.06	20.3	4.53	45.3
	slice5	10.04	21.3	4.98	47.3
	slice6	10.03	20.4	4.41	37.8
	slice7	10.03	20.5	4.87	42.9
WING 3	Slice1	10.22	20.2	5.03	45.9
	slice2	10.08	20.9	4.5	40.8
	slice3	10.14	19.8	4.89	46.8
	slice4	10.15	20.6	4.63	44.7
	slice5	10.12	20.7	4.88	47.2
	slice6	10.13	21.4	4.67	45.4
	slice7	10.1	20.7	4.97	46
	Airfoil	10	24,8	5,23	48,1

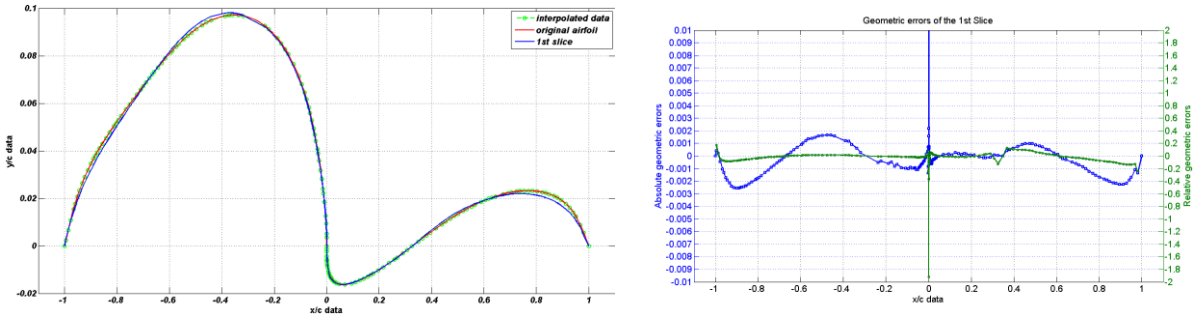

Figure 1. (a). Comparison between the geometry of the first foam wing panels' slice and the airfoil; (b). Absolute error distribution along chord (in blue) and relative error (in green).

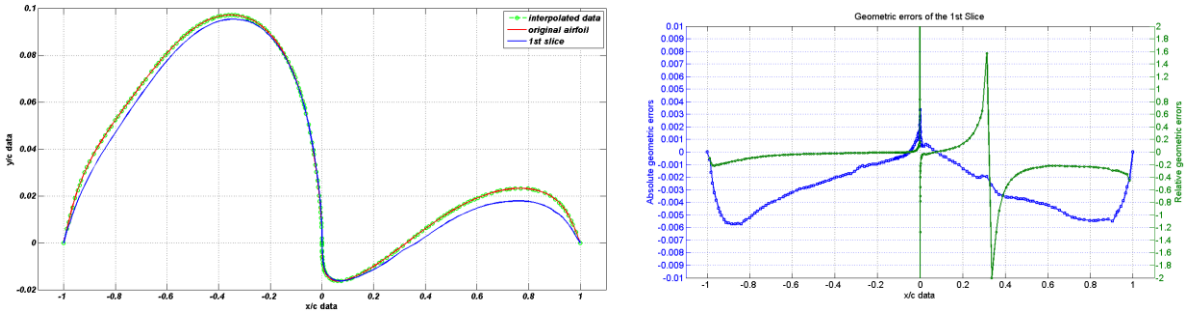

Figure 2. (a). Comparison between the geometry of the first foam covered with fiberglass wing panels' slice and the airfoil; (b). Absolute error distribution along chord (in blue) and relative error (in green).

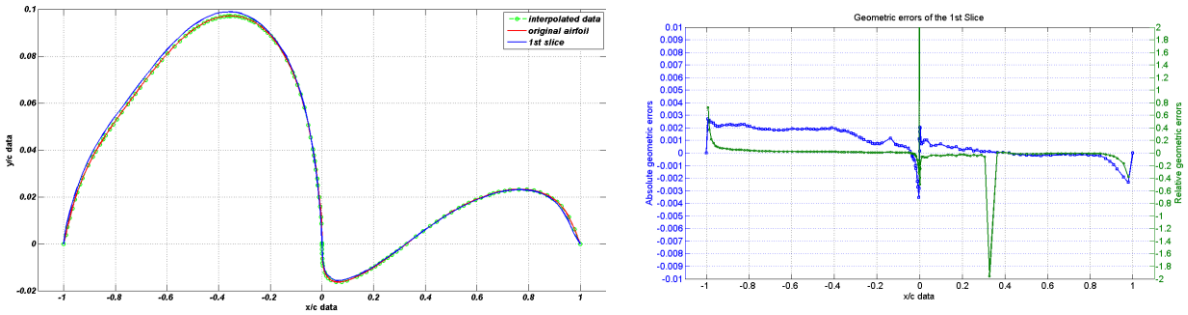

Figure 3. (a). Comparison between the geometry of the first fiberglass skin with balsa core wing panels' slice and the airfoil; (b). Absolute error distribution along chord (in blue) and relative error (in green).

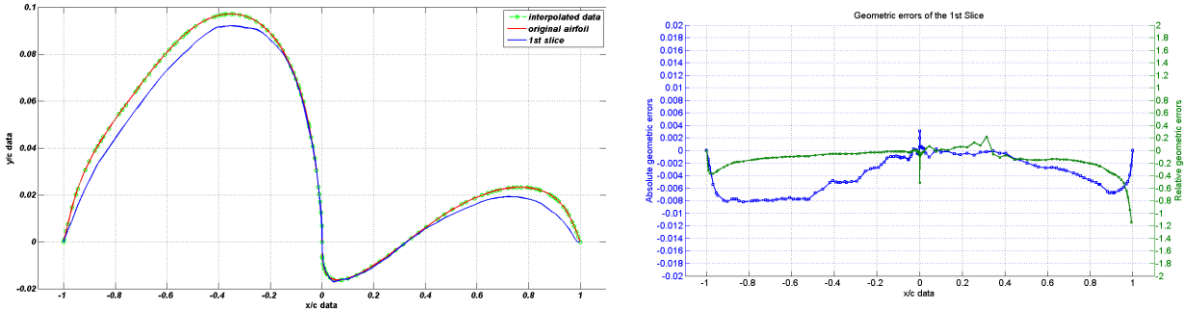

Figure 4. (a). Comparison between the geometry of the first balsa wing panels' slice and the airfoil; (b). Absolute error distribution along chord (in blue) and relative error (in green).

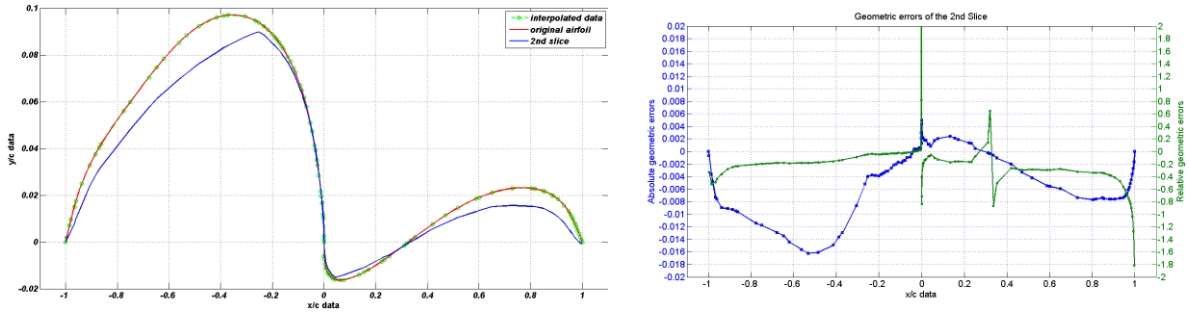

Figure 5. (a). Comparison between the geometry of the second balsa wing panels' slice and the airfoil; (b). Absolute error distribution along chord (in blue) and relative error (in green).

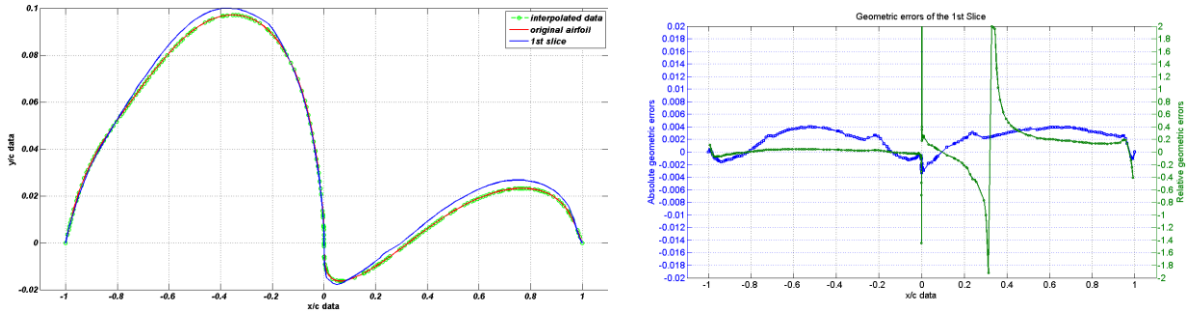

Figure 6. (a). Comparison between the geometry of the first foam and fiberglass box wing panels' slice and the airfoil; (b). Absolute error distribution along chord (in blue) and relative error (in green).

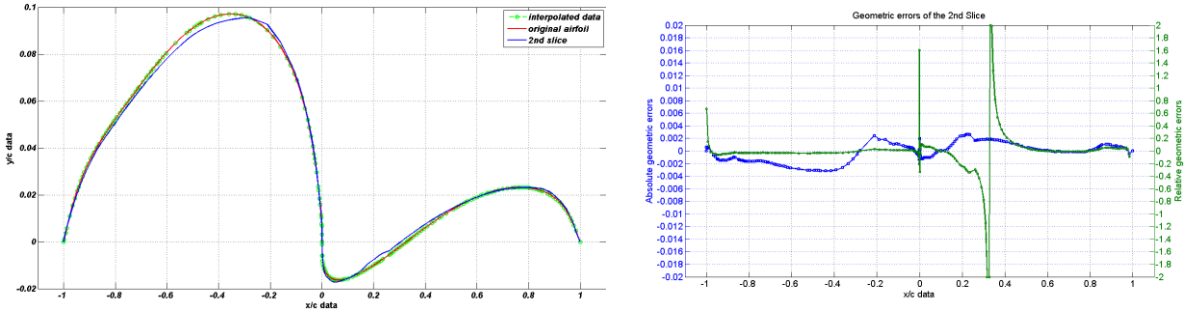

Figure 7. (a). Comparison between the geometry of the second balsa wing panels' slice and the airfoil; (b). Absolute error distribution along chord (in blue) and relative error (in green).

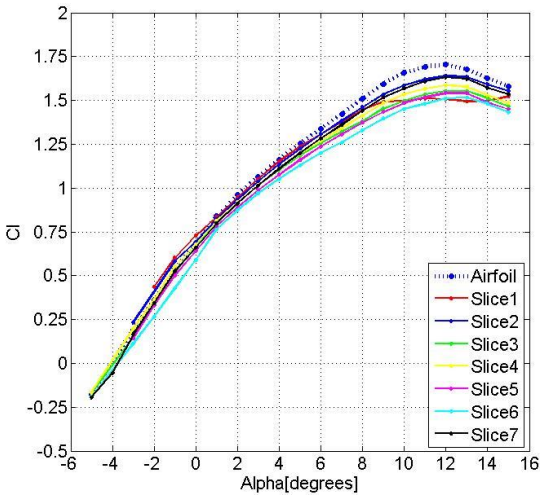

Graph 1. First foam wing panels' lift coefficient curves for Re = 140,000

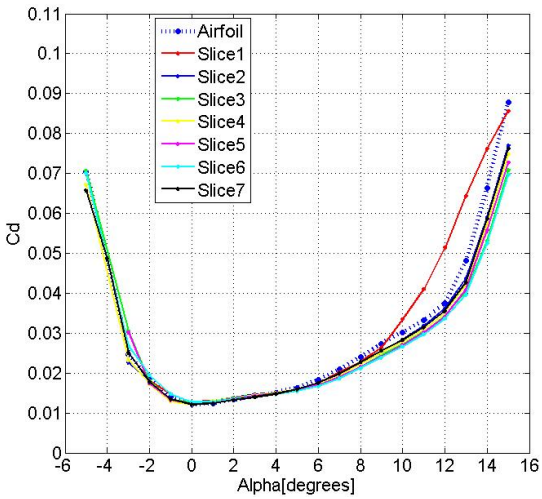

Graph 2. First foam wing panels' drag coefficient curves for Re = 140,000

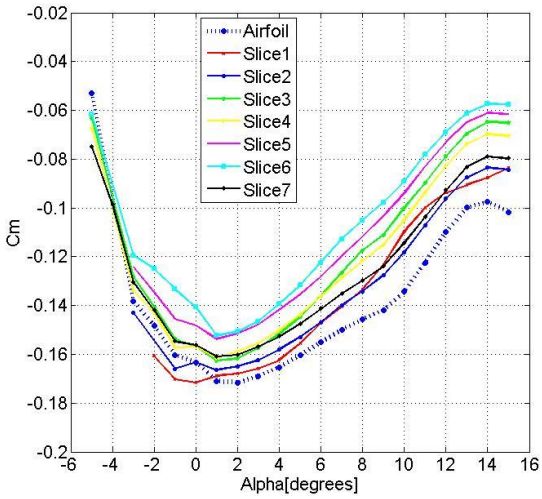

Graph 3. First foam wing panels' pitching moment coefficient curves for Re = 140,000

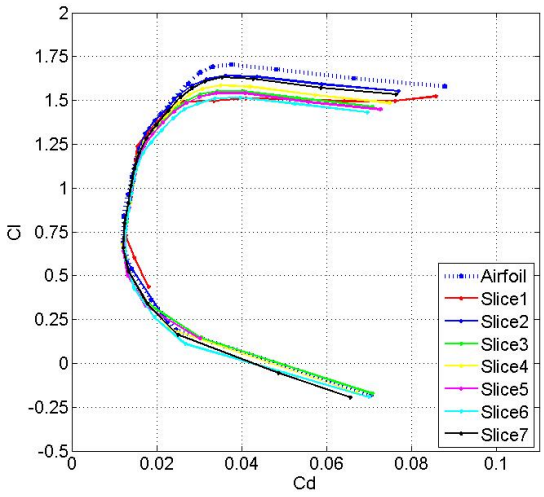

Graph 4. First foam wing panels' drag polars for Re = 140,000

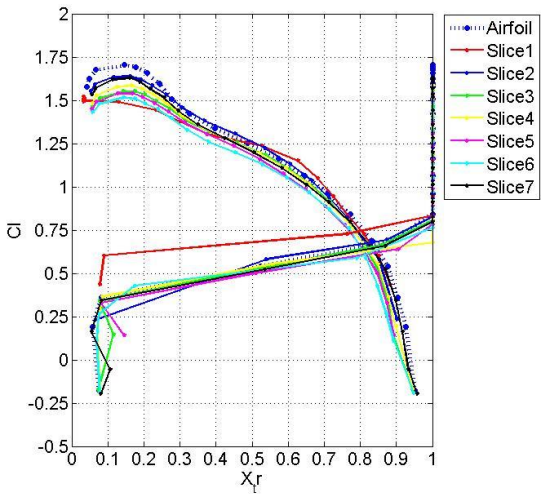

Graph 5. First foam wing panels' transition curves for Re = 140,000

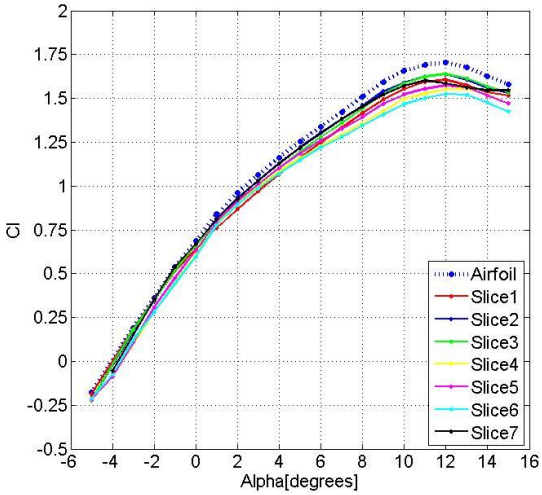

Graph 6. First foam covered with fiberglass wing panels' lift coefficient curves for Re = 140,000

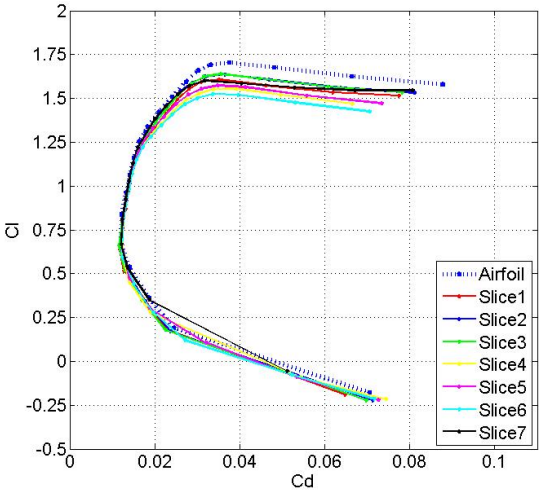

Graph 9. First foam covered with fiberglass wing panels' drag polars for Re = 140,000

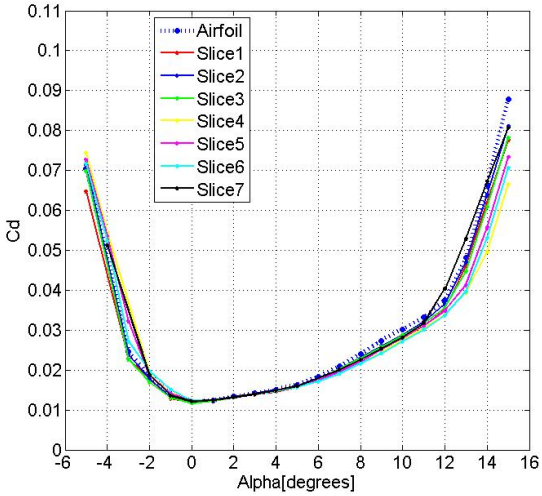

Graph 7. First foam covered with fiberglass wing panels' drag coefficient curves for Re = 140,000

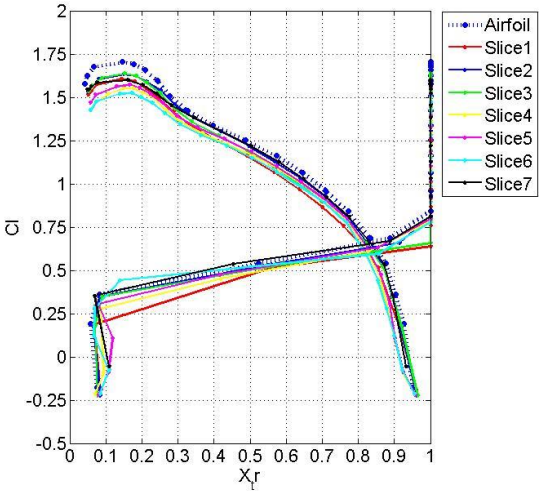

Graph 10. First foam covered with fiberglass wing panels' transition position curves for Re = 140,000

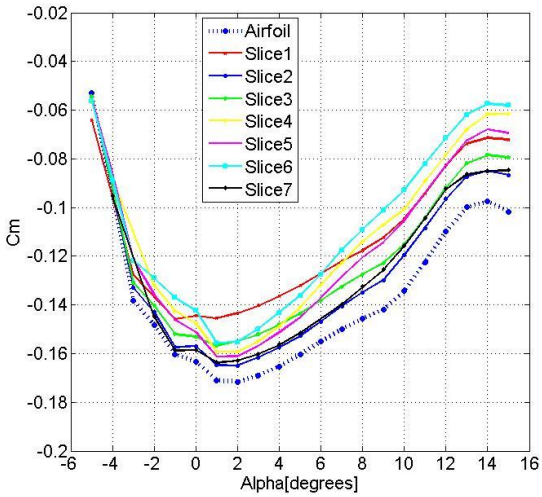

Graph 8. First foam covered with fiberglass wing panels' pitching moment coefficient curves for Re = 140,000

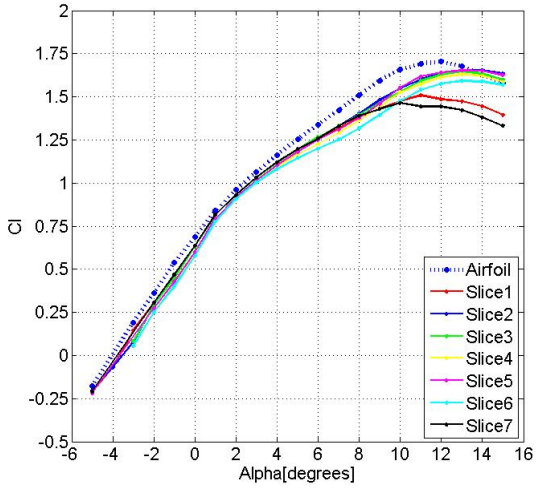

Graph 11. First fiberglass skin with balsa core wing panels' lift coefficient curves for Re = 140,000

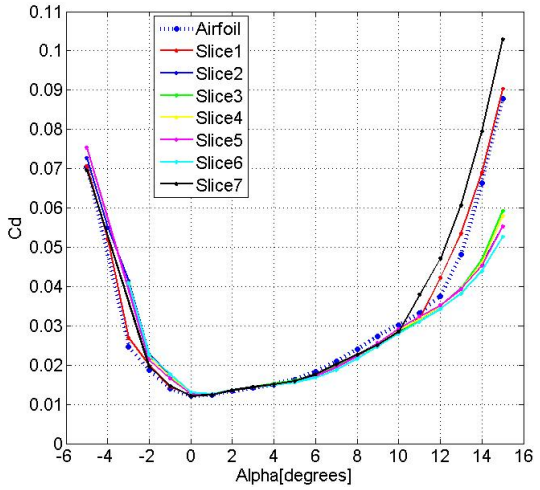

Graph 12. First fiberglass skin with balsa core wing panels' drag coefficient curves for Re = 140,000

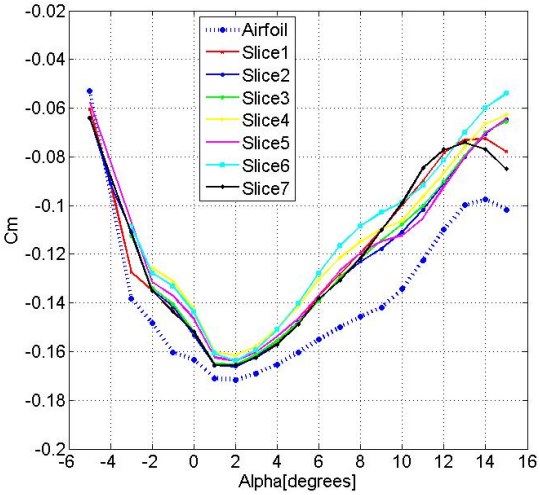

Graph 13. First fiberglass skin with balsa core wing panels' pitching moment coefficient curves for Re = 140,000

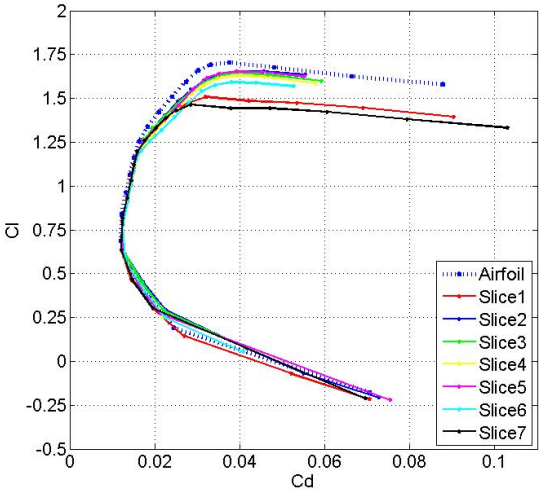

Graph 14. First fiberglass skin with balsa core wing panels' drag polars for Re = 140,000

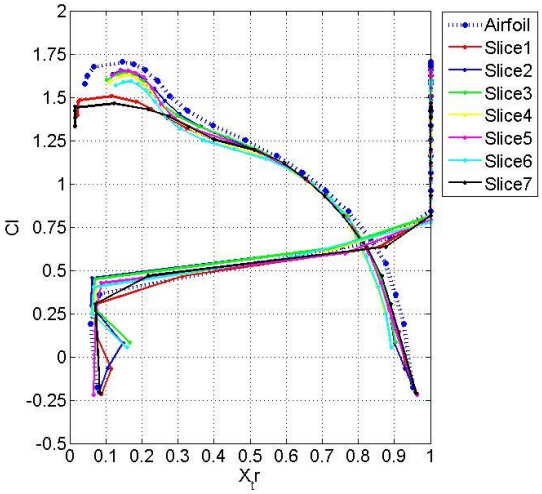

Graph 15. First fiberglass skin with balsa core wing panels' transition position curves for Re = 140,000

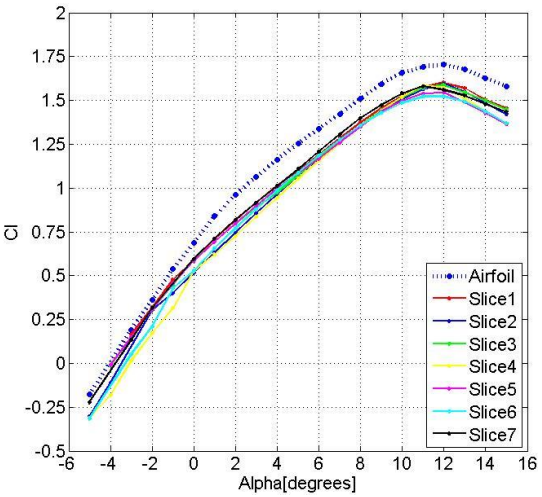

Graph 16. First balsa wing panels' lift coefficient curves for Re = 140,000

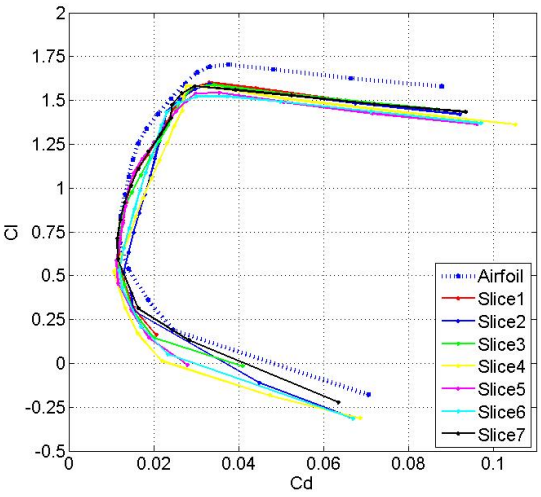

Graph 19. First balsa wing panels' drag polars for Re = 140,000

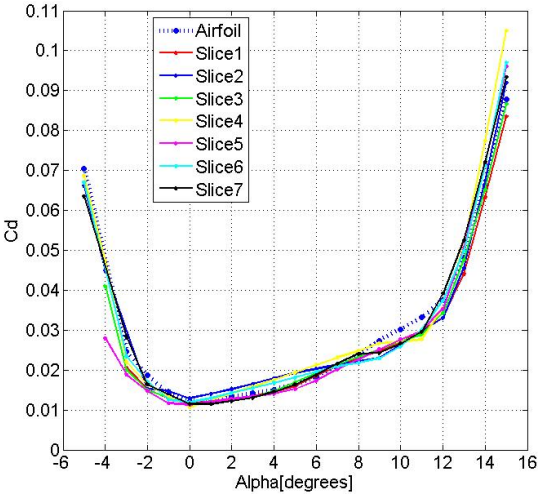

Graph 17. First balsa wing panels' drag coefficient curves for Re = 140,000

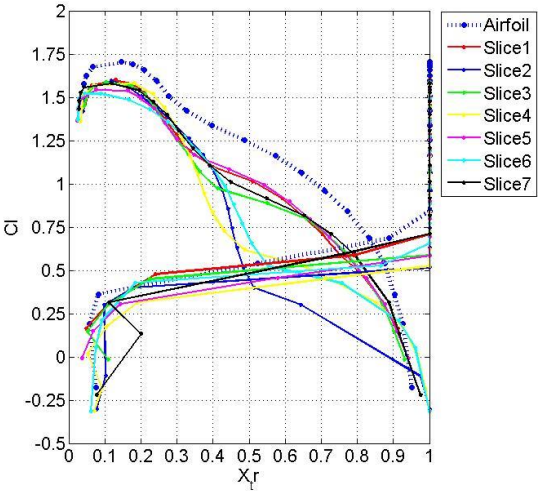

Graph 20. First balsa wing panels' transition position curves for Re = 140,000

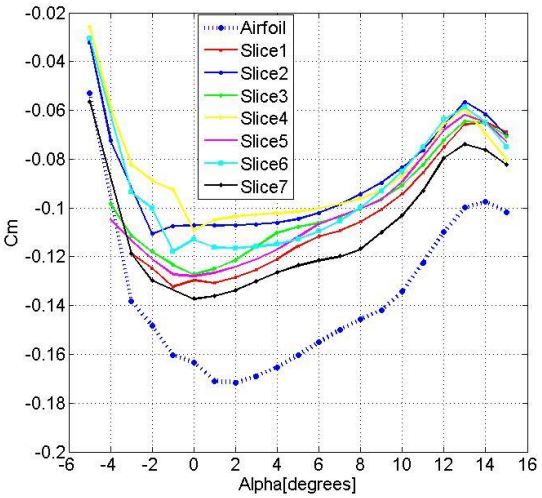

Graph 18. First balsa wing panels' pitching moment coefficient curves for Re = 140,000

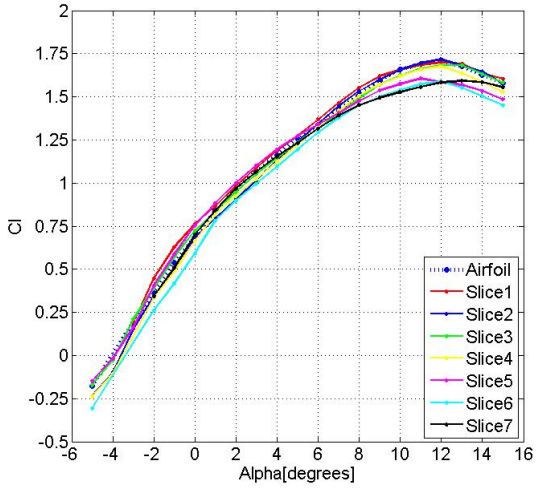

Graph 21. First foam and fiberglass box wing panels' lift coefficient curves for Re = 140,000

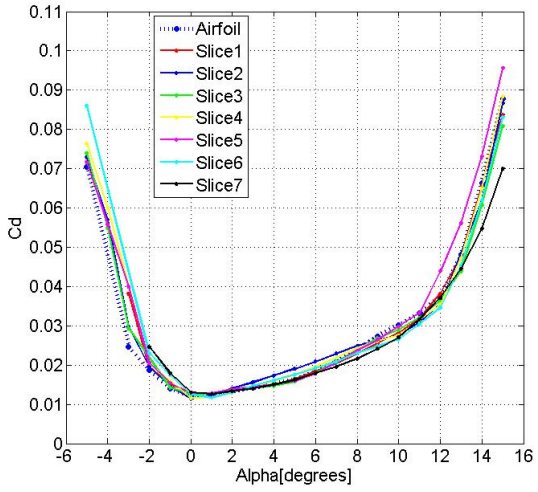

Graph 22. First foam and fiberglass box wing panels' drag coefficient curves for Re = 140,000

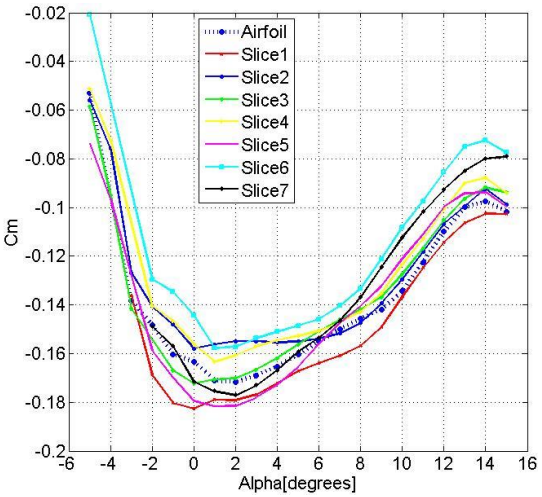

Graph 23. First foam and fiberglass box wing panels' pitching moment coefficient curves for Re = 140,000

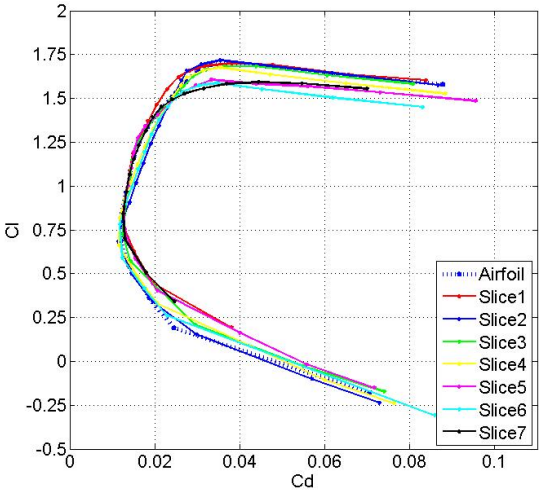

Graph 24. First foam and fiberglass box wing panels' drag polars for Re = 140,000

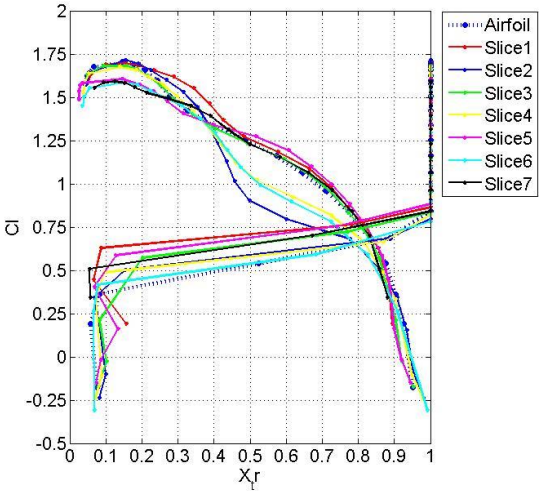

Graph 25. First foam and fiberglass box wing panels' transition position curves for Re = 140,000

Table 7 to 11. Aerodynamic average results between the three wing panels' slices of the foam, foam covered with fiberglass, fiberglass skin with balsa core, balsa, and foam and fiberglass box concepts

	Re=140.000		Re=340.000		Re=600.000	
	MEAN	AIRFOIL	MEAN	AIRFOIL	MEAN	AIRFOIL
C_{L0}	0,654	0,686	0,685	0,784	0,680	0,786
$C_{L_{max}}$	1,555	1,704	1,566	1,726	1,624	1,765
$C_{D_{min}}$	0,0120	0,0121	0,0084	0,0086	0,0073	0,0076
α_{Clmax}	12	12	12	11	14	13
Cl_{Cdmin}	0,643	0,686	0,774	0,674	0,789	0,786
$L/D)_{max}$	74,25	76,98	103,32	107,74	119,25	125,71
α_{Cdmin}	0	0	1	-1	1	0
$\alpha_{L/Dmax}$	5	4	3	3	3	3

	Re=140.000		Re=340.000		Re=600.000	
	MEAN	AIRFOIL	MEAN	AIRFOIL	MEAN	AIRFOIL
C_{L0}	0,612	0,686	0,682	0,784	0,670	0,786
$C_{L_{max}}$	1,558	1,704	1,573	1,726	1,621	1,765
$C_{D_{min}}$	0,0123	0,0121	0,0086	0,0086	0,0076	0,0076
α_{Clmax}	12	12	12	11	13	13
Cl_{Cdmin}	0,691	0,686	0,750	0,674	0,798	0,786
$L/D)_{max}$	73,40	76,98	101,61	107,74	117,46	125,71
α_{Cdmin}	0	0	1	-1	1	0
$\alpha_{L/Dmax}$	5	4	3	3	3	3

	Re=140.000		Re=340.000		Re=600.000	
	MEAN	AIRFOIL	MEAN	AIRFOIL	MEAN	AIRFOIL
C_{L0}	0,605	0,686	0,667	0,784	0,629	0,786
$C_{L_{max}}$	1,556	1,704	1,568	1,726	1,601	1,765
$C_{D_{min}}$	0,0124	0,0121	0,0089	0,0086	0,0077	0,0076
α_{Clmax}	12	12	13	11	13	13
Cl_{Cdmin}	0,731	0,686	0,751	0,674	0,813	0,786
$L/D)_{max}$	72,73	76,98	99,43	107,74	113,81	125,71
α_{Cdmin}	1	0	1	-1	2	0
$\alpha_{L/Dmax}$	5	4	3	3	3	3

	Re=140.000		Re=340.000		Re=600.000	
	MEAN	AIRFOIL	MEAN	AIRFOIL	MEAN	AIRFOIL
C_{L0}	0,636	0,686	0,599	0,784	0,598	0,786
$C_{L_{max}}$	1,635	1,704	1,608	1,726	1,655	1,765
$C_{D_{min}}$	0,0119	0,0121	0,0091	0,0086	0,0085	0,0076
α_{Clmax}	12	12	12	11	13	13
Cl_{Cdmin}	0,652	0,686	0,636	0,674	0,725	0,786
$L/D)_{max}$	71,50	76,98	94,86	107,74	108,73	125,71
α_{Cdmin}	0	0	0	-1	1	0
$\alpha_{L/Dmax}$	5	4	5	3	4	3

	Re=140.000		Re=340.000		Re=600.000	
	MEAN	AIRFOIL	MEAN	AIRFOIL	MEAN	AIRFOIL
C_{L0}	0,641	0,686	0,668	0,784	0,666	0,786
$C_{L_{max}}$	1,621	1,704	1,625	1,726	1,663	1,765
$C_{D_{min}}$	0,0117	0,0121	0,0093	0,0086	0,0086	0,0076
α_{Clmax}	12	12	12	11	12	13
Cl_{Cdmin}	0,663	0,686	0,742	0,674	0,717	0,786
$L/D)_{max}$	67,95	76,98	92,45	107,74	107,36	125,71
α_{Cdmin}	0	0	1	-1	1	0
$\alpha_{L/Dmax}$	4	4	5	3	6	3

Table 12. Best concept performance results according with different aerodynamic parameters.

Cl_0	1st - Foam	-10.5 %
	2nd - Foam with fiberglass cover	-13 %
	3th - Foam and fiberglass box	-13.9 %
	4th - Fiberglass skin with balsa core	-15.8 %
	5th - Balsa	-20.6 %
Cl_{max}	1st - Foam and fiberglass box	-5.5 %
	2nd - Balsa	-6.6 %
	3th - Foam with fiberglass cover	-8.5 %
	4th - Foam	-8.7 %
	5th - Fiberglass skin with balsa core	-9.1 %
Cl/Cd_{max}	1st -Foam	-4.4 %
	2nd - Foam with fiberglass cover	-5.8 %
	3th - Fiberglass skin with balsa core	-7.9 %
	4th - Balsa	-12.6 %
	5th - Foam and fiberglass box	-13.7 %